Published in final edited form as:

Cancer Res. 2021 February 15; 81(4): 935–944. doi:10.1158/0008-5472.CAN-20-1804.

Robust p53 stabilization is dispensable for its activation and tumor suppressor function

Ning Kon[1], **Michael Churchill**[2], **Huan Li**[1], **Siddhartha Mukherjee**[2], **James J. Manfredi**[3], **Wei Gu**[1]

[1]Institute for Cancer Genetics, Department of Pathology and Cell Biology, and Herbert Irving Comprehensive Cancer Center, College of Physicians & Surgeons, Columbia University, 1130 Nicholas Ave, New York, NY 10032, USA

[2]Department of Medicine and Herbert Irving Comprehensive Cancer Center, College of Physicians & Surgeons, Columbia University, 1130 Nicholas Ave, New York, NY 10032, USA

[3]Department of Oncological Sciences, Icahn School of Medicine at Mount Sinai, One Gustave L. Levy Place, New York, NY 10029

Abstract

p53 is a short-lived protein with low basal levels under normal homeostasis conditions. However, upon DNA damage, levels of p53 dramatically increase for its activation. Although robust stabilization of p53 serves as a 'trademark" for DNA damage responses, the requirement for such dramatic protein stabilization in tumor suppression has not been well addressed. Here we generated a mutant $p53^{KQ}$ mouse where all the C-terminal domain lysine residues were mutated to glutamines (K to Q mutations at K367, K369, K370, K378, K379, K383 and K384) to mimic constitutive acetylation of the p53 C-terminus. Due to p53 activation, $p53^{KQ/KQ}$ mice were perinatal lethal, yet this lethality was averted in $p53^{KQ/-}$ mice, which displayed normal postnatal development. Nevertheless, $p53^{KQ/-}$ mice died prematurely due to anemia and hematopoiesis failure. Further analyses indicated that expression of the acetylation-mimicking p53 mutant *in vivo* induces activation of p53 targets in various tissues without obviously increasing p53 levels. In the well-established pancreatic ductal adenocarcinoma mouse model (PDAC), expression of the acetylation-mimicking p53 mutant protein effectively suppressed K-Ras-induced PDAC tumor development in the absence of robust p53 stabilization. Together our results provide proof-of-principle evidence that p53-mediated transcriptional function and tumor suppression can be achieved independently of its robust stabilization and reveal an alternative approach to activate p53 function for therapeutic purposes.

Corresponding Author: Wei Gu, Institute for Cancer Genetics, Columbia University, 1130 St. Nicholas Ave. Rm 609A, New York, NY 10032. Phone 212-851-5282; wg8@cumc.columbia.edu.

Authors' Contributions

Conception and experimental design: N.K. and W.G. Methodology and data acquisition: N.K., M.C. and H.L. Analysis and interpretation of data: N.K., M.C., S.M., J.J.M. and W.G. Manuscript writing: N.K., J.J.M. and W.G.

COMPETING INTERESTS STATEMENT

The authors declare that they have no competing financial interests.

Introduction

p53 is a short-lived protein with very low basal levels in normal unstressed conditions and the stability of p53 is controlled predominantly by Mdm2-mediated ubiquitination and subsequent proteasome-dependent degradation (1,2). Upon DNA damage, the interaction between p53 and Mdm2 is suppressed, resulting in increasing levels of p53 protein and transcriptional activation of p53 target genes (3). Although early studies showed that Mdm2 induced p53 ubiquitination mainly at the lysine residues located at the C-terminal domain (CTD), both the levels and the activity of p53 were not significantly altered in the *p53* knock-in mice in which the lysine residues were replaced with arginine, suggesting alternative ubiquitination sites are utilized for Mdm2-mediated degradation. Notably, other posttranslational modifications, such as acetylation, methylation, neddylation, and sumoylation, also occur on the same lysine residues, and play important roles in regulating p53 transcriptional activities. p53 is one of the first non-histone proteins that were discovered to be regulated by acetylation and deacetylation (4,5). Although the physiological functions of acetylation at K120 and K164 have been elucidated using p53 acetylation-defective mice (6), the *in vivo* functions of CTD acetylation are not completely understood. Notably, by examining the phenotypes of mice lacking C-terminally truncated derivatives of p53, the role of the CTD in transcriptional regulation is further revealed. For example, Simeonova et al. have shown that homozygous mutant mice expressing $p53^{\Delta 31}$, a truncated p53 lacking the C-terminal 31 amino acids, exhibit increased p53 activity and suffer from aplastic anemia and pulmonary fibrosis (7). Hamard et al. found that the CTD regulates gene expression via multiple mechanisms, depending on the tissues and target genes (8). Both studies demonstrate that loss of the CTD results in p53 activation, suggesting that the CTD may act as a docking site for p53 transcriptional regulators. Nevertheless, the identity of theses regulators, as well as the potential regulation by CTD acetylation, needs further elucidation. Lysine acetylation often creates binding sites for “reader” proteins such as bromodomain-containing proteins. A recent study showed that PBRM1 acts as a reader for p53 acetylation on lysine 382 (K382Ac) through its bromodomain 4 (BD4) to achieve full activation of p53 targets such as p21 (9). Surprisingly, in a proteomic screen for the binding proteins of both unacetylated and acetylated p53, we have recently discovered that the acidic domain of SET acts as a new “reader” for acetylated p53 (10,11). Our study showed that the acetylation of p53 C-terminal lysine residues led to p53 activation by blocking the interactions of p53 with transcriptional corepressors such as SET without affecting p53 stability (10). However, it remains unclear whether the CTD acetylation induces tumor suppression in the absence of p53 stabilization.

The current study focused on the defects that lead to premature lethality in $p53^{KQ/-}$ mice and the tissue-specific functions of p53-KQ proteins. More importantly, to explore the potential applications in cancer therapy through the activation of p53, the tumor suppression functions, mediated by acetylation-mimicking mutant p53, was tested by expressing p53-KQ mutant in a pancreatic ductal adenocarcinoma (PDAC) mouse model (12).

Materials and Methods

Mice and pancreatic ductal adenocarcinoma model.

p53$^{KQ/+}$ mice were described previously (10). *arf* conditional knockout mice were kindly provided by Dr. Charles Sherr (12). *K-ras G12D* transgenic mice were kindly provided by Dr. Tyler Jacks. *pdx1-cre* transgenic mice and *p53* knockout mice were purchased from Jackson laboratory (13,14). Maintenance and experimental protocols using mice were approved by the Institutional Animal Care and Use Committee (IACUC) of Columbia University.

Tissue collection and immunostaining.

To determine if the mice were suffering anemia, mouse blood was collected from tail snip and a complete blood count was performed. For histopathological analysis, tissues were collected from the mice and processed according to standard procedures. For immunostaining, antibodies used in the study were: anti-mouse p53 (CM5, Novocastra), anti-cleaved Caspase3 (Cell Signaling 9661), p21 (Santa Cruz, SC397), ki67 (abcam, ab16667), and anti-WT1 (Wilms' tumor antigen 1) (Santa Cruz, sc-192). The sections were counter stained with hematoxylin.

FACS analysis of hematopoietic stem cells (HSCs) and Western blot analysis using bone marrow cells.

Bone marrow cells were collected and stained with antibodies against c-kit and Sca-1. FACS analysis was gated on Lin$^-$ cells and the cells positive for c-kit and Sca-1 were counted. For Western blot analysis, bone marrow cells were collected and the whole cell lysates were prepared with RIPA buffer. The proteins were separated by SDS-PAGE before transferred onto the membrane and probed with the indicated antibodies: anti-mouse p53 (CM5, Novocastra), anti-p21 (Santa Cruz, SX118), anti-PUMA (Santa Cruz, H-136). Levels of β-actin (Sigma) were used as total protein control.

Western blot analysis.

The whole cell extracts were prepared from mouse tissues using RIPA buffer. The whole cell extracts of spleen or thymus from an untreated wild type mouse and an irradiated (6 Gy) wild type mouse were used as controls. The proteins were then resolved by SDS-PAGE, transferred onto the membrane, and probed using the following antibodies: anti-mouse p53 (CM5, Novocastra), anti-PUMA (Santa Cruz, H-136), anti-cleaved Caspase 3 (Cell Signaling 9661), anti-p21 (Santa Cruz Biotechnology, SX118). Levels of Vinculin were used as total protein control.

Real Time PCR (RT-PCR).

The total RNA was extracted from the spleen and thymus of *p53*$^{+/-}$ and *p53*$^{KQ/-}$ mice using Trizol reagent, which was then converted to first strand cDNA by reverse transcriptase. The relative expression levels of the genes were then determined by RT-PCR using the first strand cDNAs and gene specific primers. Primers used in RT-PCR assays are: p53 forward 5'-GCAACTATGGCTTCCACCTG-3', p53 reverse 5'-

TTATTGAGGGGAGGAGAGTACG-3', mdm2 forward 5'-GACTCGGAAGATTACAGCC-TGA-3', mdm2 reverse 5'-TGTCTGATAGACTGTGACCCG-3', p21 forward 5'-AGATCCACAGCGATATCCAGAC-3', p21 reverse 5'-ACCGAAGAGACAACGGCA CACT-3', p27 forward 5'-GACAATCAGGCTGGGTTAGC-3', p27 reverse 5'-TTCTG TTGGCCCTTTTGTTT-3', ccng1 forward 5'-CGTGTCCTCAGTTCTTTGGCTTTGACA CG-3', ccng1 reverse 5'-GATGCTTCGCCTGTACCTTCATT-3', pml forward 5'-CCAGCGTCCTGCCACAGT-3', pml reverse 5'-GGTGCGATATGCATTCAGTAACTC-3', noxa forward 5'-TCGCAAAAGAGCAGGATGAG-3', noxa reverse 5'-CACTTTGTCT CCAATCCTCCG-3, puma forward 5'-ACGACCTCAACGCGCAGTACG-3', puma reverse 5'-GAGGAGTCCCATGAAGAGATTG-3', bax forward 5'-CAGGATGCGTCC-ACCAAGAA-3', bax reverse 5'-AGTCCGTGTCCACGTCAGCA-3', DR5 forward 5'-CGGGCAGATCACTACACCC-3', DR5 reverse 5'-TGTTACTGGAACAAAGACAGCC-3', Bim forward 5'-GGAGACGAGTTCAACGAAACTT-3', Bim reverse 5'-AACAGTTGTAA GATAACCATTTGAGG-3', Gadd45a forward 5'-CCGAAAGGATGGACACGGTG-3', Gadd45a reverse 5'-TTATCGGGGTCTACGTTGAGC-3', and β-actin forward 5'-GGC TGTATTCC-CCTCCATCG-3', β-actin reverse 5'-CCAGTTGGTAACAATGCCATGT-3'.

Statistical analysis.

Results are shown as means +/− S.D. Statistical significance was determined by using a two-tailed, unpaired Student *t*-test. The survival curves were analyzed using a two-tailed, unpaired Student t-test or Log-rank (Mantel-Cox) Test for survival curves by Prism software.

Results

The lethality of the *p53$^{KQ/KQ}$* mice was completely averted in *p53$^{KQ/-}$* mice.

To identify the precise roles of acetylation in the activation of p53, we generated an acetylation-mimic mutant *p53-KQ* mouse in which all seven C-terminal acetylated lysine residues were mutated to glutamines because glutamine resembles acetylated lysine. The *p53$^{KQ/KQ}$* mice died at birth due to the developmental defects in the brain and their inability to obtain nourishment (10). To obtain live mice expressing only mutant p53-KQ proteins, *p53-KQ* heterozygote (*p53$^{KQ/+}$*) mice were crossed with *p53* heterozygote knockout (*p53$^{+/-}$*) mice to determine if live *p53$^{KQ/-}$* mice can be obtained as a result of reduced levels of mutant p53-KQ protein and decreased p53-mediated transcription in *p53$^{KQ/-}$* mice. Pups were genotyped when they were one week old, and the genotype distribution was observed close to the expected Mendelian frequency (Supplementary Table S1). These results indicated that, unlike the *p53$^{KQ/KQ}$* mice, that died shortly after birth, *p53$^{KQ/-}$* mice survived during early postnatal development. Interestingly, the footpads and tails of *p53$^{KQ/-}$* mice appeared darker than those of the *p53$^{+/-}$* mice due to hyperpigmentation (Fig. 1A, Supplementary Fig. S1A). This phenotype is reminiscent of a similar hyperpigmentation observed in other mutant p53 mouse models with increased p53 activation (7,8,15), consistent with our previous finding that p53-KQ proteins have elevated transcriptional activities (10). These data indicate that the perinatal lethality of the *p53$^{KQ/KQ}$* mice can be completely averted by the loss of one *p53-KQ* allele in *p53$^{KQ/-}$* mice.

p53$^{KQ/-}$ mice died prematurely partially due to anemia and hematopoiesis failure.

Although *p53*$^{KQ/-}$ mice had normal postnatal development, most of *p53*$^{KQ/-}$ mice showed reduced body weight and decreased physical activities after a few weeks compared to the control littermates (Fig. 1B). Eventually, *p53*$^{KQ/-}$ mice became lethargic with accelerated breathing, and died prematurely with a median survival of 35 days (Fig. 1C). To determine the cause of premature lethality, weaning age *p53*$^{KQ/-}$ mice were dissected to reveal an enlarged heart, smaller thymus, and pale color in many blood rich organs such as liver and kidney compared to those of the *p53*$^{+/-}$ littermates (Fig. 1D). Particularly, the enlarged heart and pale blood color (Supplementary Fig. S1B), which are often associated with chronic blood loss and anemia, prompted us to perform a complete blood cell count using 3-week-old mice (10 each of *p53*$^{+/-}$ and *p53*$^{KQ/-}$ mice). The results showed that there was a significantly reduced blood-cell count in red blood cells and white blood cells in *p53*$^{KQ/-}$ mice, compared to those in *p53*$^{+/-}$ littermates (Fig. 1E). In particular, the number of red blood cells was reduced by 80% in *p53*$^{KQ/-}$ mice, consistent with the pale blood color in these mice. The number of white blood cells was also reduced by more than 50%, and the number of the platelets was reduced by 30% in *p53*$^{KQ/-}$ mice. Furthermore, the sections of the bones from morbid-bound *p53*$^{KQ/-}$ mice displayed a dramatic loss of bone marrow cells, compared to those from the *p53*$^{+/-}$ littermates (Fig. 1F, **panel 2** vs. **1**). Thus far, since these mice died at relatively young ages, we have not observed crunch back or grey hair associated with aging in mutant mice. Taken together, these findings indicate that *p53*$^{KQ/-}$ mice suffered from anemia and hematopoiesis failure.

Further characterization of bone marrow in *p53*$^{KQ/-}$ mice.

To understand the details of the loss of bone marrow cells in *p53*$^{KQ/-}$ mice, the femurs from postnatal days 6 (P6), P14, and P28 were sectioned and stained with hematoxylin and eosin (H&E staining) (Supplemental Fig. S2A). There was no obvious difference in the bone marrow between *p53*$^{KQ/-}$ and *p53*$^{+/-}$ mice at P6 (Supplemental Fig. S2B, panel 3 vs. 1), whereas the bone marrow cells appeared much less in *p53*$^{KQ/-}$ mice than in *p53*$^{+/-}$ mice at P14 (Fig. 2A, **panel 5** vs. **1**). By P28, there were only a few cells left in the bone marrow from *p53*$^{KQ/-}$ mice, (Fig. 2A, **panel 13** vs. **9**). These results suggested that although the hematopoiesis was adequate at early postnatal stages, there was a progressive loss of bone marrow cells and the hematopoiesis eventually failed in *p53*$^{KQ/-}$ mice. Since the skin hyperpigmentation in *p53*$^{KQ/-}$ mice indicated increased p53 transcriptional activities in *p53*$^{KQ/-}$ mice, it is critical to determine whether the loss of bone marrow cells is due to p53 activation and increased expression of p53 target genes. To this end, immunostaining was performed using bone sections. There was no obvious difference in p53 staining in bone marrow cells from *p53*$^{KQ/-}$ mice compared to those of the *p53*$^{+/-}$ mice, suggesting that the abundance of p53 was not affected by the C-terminal K to Q mutations in p53 (Fig. 2A, **panel 6** vs. **2**, and **panel 14** vs. **10**). The was no significant staining of cleaved Caspase 3 in bone marrow from the *p53*$^{KQ/-}$ mice and the control mice, indicating that the loss of bone marrow cells in *p53*$^{KQ/-}$ mice was not due to apoptotic cell death. Next, to determine if the loss of bone marrow cells is due to reduced cell proliferation, the immuno-staining of p21 (cdkn1a), an important target in p53-mediated cell growth arrest, was performed. Indeed, there was increased staining of p21 in the bone marrow cells from P14 and P28 *p53*$^{KQ/-}$

mice (Fig. 2A, **panel 7** vs. **3**, and **panel 15** vs. **11**), indicating that p21 expression was induced in $p53^{KQ/-}$ mice. To determine if the cell proliferation was affected by the increased expression of p21, immunostaining of ki67 was performed on bone sections. There was modest reduction of ki67-positive cells in the P6 bones from $p53^{KQ/-}$ mice compared to the control mice (Supplemental Fig. S2B, panel 4 vs. 2). By P14, accompanying the loss of bone marrow cells, the ki67-positive cells were also reduced (Fig. 2A, **panel 8** vs. **4**). Notably, while many proliferating cells were in the cancellous (spongy) bone of the $p53^{+/-}$ mice at P28, there were almost no ki67-positive cells in the cancellous bone in $p53^{KQ/-}$ mice (Fig. 2A, **panel 16** vs. **12**). Taken together, these results suggest that although there were no noticeable changes of p53 abundance due to the C-terminal K-to-Q mutations, one *p53-KQ* allele is sufficient to promote p21 expression, and cause growth arrest in bone marrow cells and bone marrow failure in $p53^{KQ/-}$ mice.

Loss of hematopoiesis stem cells in $p53^{kq/-}$ mice.

Next, we examined whether the hematopoiesis failure was due to defects in hematopoietic stem cells (HSCs) in $p53^{KQ/-}$ mice. To this end, bone marrow cells were collected from femurs of the P6 mice, and the population of the HSCs was quantitated by flow cytometry, Fluorescent Activated Cell Sorting (FACS), analysis. Both the short-term HSCs (STHSCs) and the long-term HSCs (LTHSCs) were reduced in $p53^{KQ/-}$ mice compared to those of the control mice (Fig. 2B). The STHSCs ($Lin^{-}Sca\text{-}1^{+}c\text{-}Kit^{+}$) decreased from 0.34% in $p53^{+/-}$ mice to 0.0034% in $p53^{KQ/-}$ mice, whereas LTHSCs ($Lin^{-}Sca\text{-}1^{+}c\text{-}Kit^{+}$ $CD150^{+}$), a subpopulation of the STHSCs, decreased from 10.1% of the STHSCs in $p53^{+/-}$ mice to 0% in $p53^{KQ/-}$ mice (Supplementary Table S2A). To determine if the hematopoietic defects occurred earlier, the FACS analysis was also performed on liver cells from embryos at embryonic day 18.5 (E18.5). Consistent with the reduction of HSCs at P6, STHSCs decreased from 3.50% in $p53^{+/-}$ embryos to 1.29% in $p53^{KQ/-}$ embryos, whereas LTHSCs decreased from 14.8% of the STHSCs in $p53^{+/-}$ embryos to 0.77% in $p53^{KQ/-}$ embryos (Supplementary Table S2B). Interestingly, several studies have also implicated the critical roles of p53 in stem cell differentiation and future research is required to understand the detail mechanisms of how p53-KQ affects stem cell development in mice (16,17). These results demonstrate that the hematopoiesis failure in $p53^{KQ/-}$ mice was caused by the progressive depletion of HSCs.

Loss of stem cells in the testis of $p53^{KQ/-}$ mice.

Besides the hematopoiesis failure, the testes appeared much smaller in $p53^{KQ/-}$ mice compared to those of the control mice (Fig. 1C). We proceeded to investigate the testes from the three-week-old mice to determine the underlying abnormalities in $p53^{KQ/-}$ mice. Typically, spermatogonia are the stem cells of the male reproductive system and are located just beneath the basement membrane of seminiferous tubules. Proliferation of spermatogonia results in self-renewal and production of spermatocytes and sperms through meiosis and mitosis. Another important type of cells in testes is Sertoli cells, which are non-dividing somatic cells to support the development and maturation of sperm cells. In three-week-old $p53^{+/-}$ mice, both spermatogonia (Fig. 2C1 *) and Sertoli cells (Fig. 2C1 <) can be observed after H&E staining. The developing spermatocytes also can be observed (Fig. 2C1). To distinguish Sertoli cells from the cells involved in spermatogenesis, immunostaining was

performed using an antibody against Wilms' tumor antigen (WT1) because only Sertoli cells are labeled by the anti-WT1 antibody in the testes (18). As expected, there were abundant spermatogonia and spermatocytes (WT1-staining-negative cells with blue-colored nuclei from hematoxylin counter staining) and Sertoli cells (WT1-staining-positive cells with brown-colored nuclei) in the testis of $p53^{+/-}$ mice (Fig. 2C2). In contrast, most of the cells present in the seminiferous tubules in three-week-old $p53^{KQ/-}$ mice displayed diffused hematoxylin staining consistent to that of Sertoli cells (Fig. 2C3), and most of them were positive for WT1 staining (Fig. 2C4). There were very few spermatogonia indicated by the negative WT1-staining (cells with blue-colored nuclei), suggesting that spermatogonia failed to undergo self-renewal and differentiation in $p53^{KQ/-}$ mice (Fig. 2C4). Further analyses of testes from earlier days showed that defects in spermatogenesis occurred as early as P14 (Supplementary Fig. S3, panel 15 vs. 7), whereas little differences were observed in the testes at P5 from $p53^{KQ/-}$ mice compared to those of the control mice (Supplementary Fig. S3, panel 11 vs. 3). In addition, no obvious p53 staining and cleaved Caspase 3 staining were observed in the testes at P5 and P14 from either $p53^{+/-}$ or $p53^{KQ/-}$ mice (Supplementary Fig. S3, panels 10 and 14 vs. 2 and 6; panels 12 and 16 vs. 4 and 8, respectively). Taken together, these results suggest that along with the HSCs, the spermatogenic stem cells were also affected by p53 activation in $p53^{KQ/-}$ mice.

p53 activation in $p53^{KQ/-}$ mice without robust p53 stabilization

To examine the molecular changes in bone marrow cells, the expression levels of p53 and p53 target genes were determined by Western blotting using whole cell extracts of the bone marrow cells from P6 mice (Fig. 3A). As a control, the whole cell extracts from wild type thymus and thymus from ionizing radiation (IR) treated wild type mouse were included in the Western blot analysis to show the expression of p53 and its target genes p21 and PUMA. As expected, the levels of p53 were markedly increased in wild type thymus after IR treatment (Fig. 3A, **lane 2** vs. **1**). As a result, the levels of p53 target genes, p21 and PUMA, were also induced in the thymus from IR-treated wild type mouse compared to those of the control mouse (Fig. 3A, **lane 2** vs. **1**). There was no robust stabilization of p53 in the bone marrow cells from both $p53^{+/-}$ and $p53^{KQ/-}$ mice (Fig. 3A, **lane 3** and **4**), indicating that the expression levels of p53 were very low. Nevertheless, the levels of p21 and PUMA in $p53^{KQ/-}$ mice were markedly increased, compared to those of $p53^{+/-}$ mice (Fig. 3A, **lane 4** vs. **3**). Similar results were also obtained in bone marrow cells from P14 mice. Although the levels of p53 were indeed much lower in bone marrow cells than those in the wild type spleen (Supplementary Fig. S4A, lanes 3 and 4 vs. 1 and 2), there were similar protein levels of p53 in bone marrow cells from $p53^{+/-}$ and $p53^{KQ/-}$ mice (Supplementary Fig. S4A, lanes 3 and 4). In contrast, the levels of p21 were markedly higher in $p53^{KQ/-}$ mice than in $p53^{+/-}$ mice, consistent with the results in bone marrow cells form P6 mice (Supplementary Fig. S4A, lane 4 vs. 3). Moreover, high levels of p21 were also detected in the liver from E13.5 $p53^{KQ/-}$ embryos, but not from $p53^{+/-}$ embryos (Supplementary Fig. S4B, lanes 2 and 3 vs. 1), without obvious differences in the protein levels of p53 (Supplementary Fig. S4B, lanes 1–3). In contrast, p21 expression was not detected in fetal spleen from either mutants likely because hematopoiesis occurs mainly in liver, but not in spleen, during embryonic development (Supplementary Fig. S4B lanes 4–6). Taken together, these results indicate that

activation of p53 function plays an important role in regulating hematopoiesis in $p53^{KQ/-}$ mice in the absence of robust p53 stabilization

To further demonstrate the increased expressions of p53 target genes in $p53^{KQ/-}$ mice, whole cell extracts were prepared from spleen (Fig. 3B **lanes 3** and **4**) and thymus (Fig. 3B **lanes 5** and **6**). The proteins were separated by SDS-PAGE prior to Western blot analysis. As a control, the splenic protein extracts from a wild type mouse (Fig. 3B **lane 1**) and an IR-treated wild type mouse (Fig. 3B **lane 2**) were used to show the expressions of p53, p21, and PUMA. As expected, the levels of p53 increased dramatically in the spleen in response to IR treatment (Fig. 3B, **lane 2** vs. **1**). The levels of p21 and PUMA were also increased as a result of p53 activation (Fig. 3B, **lane 2** vs. **1**). Furthermore, apoptosis was induced in the IR-treated spleen, indicated by the presence of cleaved Caspase 3 (Fig. 3B, **lane 2** vs. **1**). In comparison, there was no obvious difference in the protein levels of p53 between $p53^{KQ/-}$ and $p53^{+/-}$ mice, in both spleens and thymi (Fig. 3B, **lane 4** vs. **3**; **lane 6** vs. **5**), suggesting that p53 is activated in p53-KQ mice without robust stabilization. In contrast, the expression levels of p21 were markedly increased in the spleen from $p53^{KQ/-}$ mice compared to the spleen from $p53^{+/-}$ mice (Fig. 3B **lane 4** vs. **3**). There was no detectable expression of p21 in thymus from either $p53^{KQ/-}$ mice or $p53^{+/-}$ mice (Fig. 3B, **lane 6** vs. **5**). Similarly, there was a modest increase of the levels of PUMA in the spleen (Fig. 3B **lane 4** vs. **3**, long exposure) and in the thymus (Fig. 3B **lane 4** vs. **3**, short exposure) from $p53^{KQ/-}$ mice, compared to $p53^{+/-}$ mice. Taken together, these results demonstrated that the expression of p53 target genes, p21 and PUMA, was induced due to the enhanced transcriptional activities of p53-KQ mutant. Notably, there was a dramatic reduction of ki67 staining in the red pulp of the spleen from $p53^{KQ/-}$ mice compared to that of the control mice (Supplementary Fig. S5, panel 4 vs. 2), suggesting that p53 activation induces cell growth arrest. Finally, there was a modest increase of the levels of cleaved Caspase 3 in the thymus from $p53^{KQ/-}$ mice compared to $p53^{+/-}$ mice, indicating apoptotic activities in the thymus of $p53^{KQ/-}$ mice (Fig. 3B, **lane 6** vs. **5**). Although the levels of p53 remain the same between $p53^{+/-}$ and $p53^{KQ/-}$ mice in those tissues, we observed much higher basal levels of p53 protein in the thymus than in the spleen (Fig. 3B). Although future investigation is required, it is possible that both p53 levels and tissue-specific cofactors play important roles in tissue-specific activation of p53 targets.

Next, we examined whether p53 can be further activated in p53-KQ mice upon DNA damage. As expected, the protein levels of p53 increased after DNA damage in both $p53^{+/-}$ and $p53^{KQ/-}$ mice (Supplementary Fig. S6, lanes 3 and 4 vs. 1 and 2). Under unstressed conditions, the levels of p21 and PUMA were higher in $p53^{KQ/-}$ mice than those in $p53^{+/-}$ mice (Supplementary Fig. S6, lane 2 vs. 1), and they were further increased in $p53^{KQ/-}$ mice after IR (Supplementary Fig. S6, lane 4 vs. 2). These results demonstrate that p53 can be stabilized and further activated in *p53-KQ* mice upon DNA damage.

To further reveal the increased expression of p53 target genes in $p53^{KQ/-}$ mice, real-time PCR (RT-PCR) assays were performed using RNA samples prepared from the spleen (Fig. 3C) and thymus (Fig. 3D). Consistent with the increased p53 transcriptional activities in $p53^{KQ/-}$ mice, many of the p53 target genes were upregulated in $p53^{KQ/-}$ mice compared to those in $p53^{+/-}$ mice. In particular, the relative mRNA levels of *p21* were increased more

than 70-fold in the spleen of $p53^{KQ/-}$ mice compared to $p53^{+/-}$ mice, the most among all the tested genes (Fig. 3C). Another cell cycle regulator *ccng1*, as well as apoptosis-associated genes, such as *puma*, were also significantly upregulated in the spleen (Fig. 3C). In thymus, the activated genes in $p53^{KQ/-}$ mice were mostly apoptosis-associated genes, such as *puma* and *noxa* (Fig. 3D). Together, these results further validate that p53 is activated in different tissues of $p53^{KQ/-}$ mice in the absence robust p53 stabilization.

Expression of p53-KQ mutant leads to effective suppression of tumor development in a pancreatic ductal adenocarcinoma mouse model.

Because of the enhanced transcriptional activities of p53-KQ mutant, we wanted to test whether the targeted expression of *p53-KQ* in tumor cells would also cause inhibition of cell growth and suppression of tumor formation. However, because the expression of *p53-KQ* during embryonic development causes neonatal lethality in $p53^{KQ/KQ}$ mice, it is not feasible to constitutively express p53-KQ proteins and observe the effects of p53-KQ proteins on tumor formation in adult mice (Supplementary Fig. S7A). However, during the course of generating *p53-KQ* mice, we noticed that the homozygote mice of the neomycin-cassette-containing *p53-KQ* allele, which is designated as *p53-KQneo* (Supplementary Fig. S7B), were alive and appeared normal for more than a year. Analysis of p53 mRNA showed that the presence of the neomycin cassette prohibited the splicing between exons 10 and 11 (Supplementary Fig. S7B). The ensuing translation of the exon 11-unspliced *p53* transcript produced a C-terminal truncated p53 that lacked the last 23 amino acids and all seven K to Q mutations due to a stop codon next to the exon 10 in the unspliced RNA (Supplementary Fig. S7B). Notably, none of the *p53-KQneo* homozygote mice had hyperpigmentation on their footpads, suggesting that the C-terminal truncated p53 does not cause increased transcriptional activities at basal levels. Importantly, the *p53-KQneo* allele allowed for conditional expression of the p53-KQ protein after excision of the neomycin cassette in the presence of tissue-specific Cre, thus avoiding the lethality when *p53-KQ* is expressed constitutively in mice (Fig. 4A).

To study the effects of the expression of p53-KQ proteins on tumor formation, we used an established pancreatic ductal adenocarcinoma (PDAC) mouse model in which tumor formation was due to tissue specific expression of oncogenic mutant K-ras G12D in pancreas in the presence of *pdx1-cre* (13). The latency of PDAC resulted from expression of K-ras G12D alone was more than six months (Fig. 4B **black line**). However, PDAC formation was accelerated when tumor suppressor *arf* was deleted, indicated by the significantly shortened life span of $arf^{fl/fl}$/$K\text{-}ras^{G12D}$/*pdx1-cre* mice compared to that of the $K\text{-}ras^{G12D}$/*pdx1-cre* mice (Fig. 4B, **red line** vs. **black line**). More importantly, because ARF inhibits Mdm2 activity upon the expression of oncogenes (19–21), Mdm2 will likely maintain its activity in the absence of ARF even when K-ras G12D is expressed. Thus, simultaneous deletion of *arf* and expression of mutant p53 allows us to test p53 tumor suppression functions without p53 stabilization.

To test the effects of p53-KQ mutant on PDAC formation, two cohorts were established: one is the control consisting of $arf^{fl/fl}$/$K\text{-}ras^{G12D}$/*pdx1-cre* mice, and the other one is the subject of the study consisting of $p53^{KQneo/KQneo}$/$arf^{fl/fl}$/$K\text{-}ras^{G12D}$/*pdx1-cre* mice. The tumor-free

survival of these cohorts was then compared to determine the effects of the expression of p53-KQ mutant on tumor formation in the PDAC mouse model. The combined expression of *K-ras G12D* oncogenic mutant and homozygote deletion of *arf* greatly accelerated the progression of PDAC and those mice developed tumors as early as one month after birth. As shown by the Kaplan-Meier plot, the 50% tumor-free survival of $arf^{fl/fl}$/K-ras^{G12D}/*pdx1-cre* mice is 66 days (Fig. 4B **red line**), whereas the mice expressing oncogenic *K-ras G12D* developed early stages of PDAC after more than six months, none dying before six months (Fig. 4B **black line**). The pancreas from $arf^{fl/fl}$/K-ras^{G12D}/*pdx1-cre* mice consisted mostly proliferating ductal cells with almost no acinar cells due to extensive proliferation of the ductal cancerous cells in the pancreas of $arf^{fl/fl}$/K-ras^{G12D}/*pdx1-cre* mice compared to the wild type mice and K-ras^{G12D}/*pdx1-cre* mice (Fig. 4C, **panel 3** vs. **1 and 2**). Upon expression of p53-KQ mutant, the median survival of mice with PDAC improved from 66 days for $arf^{fl/fl}$/K-ras^{G12D}/*pdx1-cre* mice to 143 days for $p53^{KQneo/KQneo}$/$arf^{fl/fl}$/K-ras^{G12D}/*pdx1-cre* mice ($p<0.0001$) (Fig. 4B, **red line** vs. **blue line**). The pancreas from $p53^{KQneo/KQneo}$/$arf^{fl/fl}$/K-ras^{G12D}/*pdx1-cre* mice had early stages of PDAC and the expansion of ductal cells was less extensive compared to $arf^{fl/fl}$/K-ras^{G12D}/*pdx1-cre* mice (Fig. 4C, **panel 4** vs. **3**). There were also a large number of acinar cells in the pancreas of $p53^{KQneo/KQneo}$/$arf^{fl/fl}$/K-ras^{G12D}/*pdx1-cre* mice (Fig. 4C, **panel 4**). Taken together, these results suggested that the expression of p53-KQ mutant significantly reduced tumor formation in the PDAC mouse model. As expected, K-ras expression led to upregulation of p53 protein levels in pancreas tissues ($p53^{+/+}$/K-ras^{G12D}/*pdx1-cre* mice (lane 2 vs. lane 1, Figure 4D) but this upregulation was abrogated upon the loss of ARF ($p53^{+/+}$/$arf^{fl/fl}$/K-ras^{G12D}/*pdx1-cre* mice) (lane 3 vs. lane 2, Figure 4D), resulting in tumor prone phenotypes in $p53^{+/+}$/$arf^{fl/fl}$/K-ras^{G12D}/*pdx1-cre* mice. Notably, although there was no obvious difference of the p53 levels between $p53^{KQneo/KQneo}$/$arf^{fl/fl}$/K-ras^{G12D}/*pdx1-cre* mice and $p53^{+/+}$/$arf^{fl/fl}$/K-ras^{G12D}/*pdx1-cre* mice (Figure 4D, lanes 4 and 3), the levels of p21 and PUMA were much higher in the mice expressing p53-KQ than in the mice expressing wild type p53 (Figure 4D, lane 4 vs. 3). Taken together, these results suggest that activation of p21 and PUMA induced by p53-KQ proteins is able to compensate the loss of ARF and induces tumor suppression functions without robust p53 stabilization.

Discussion

By using the acetylation-mimicking *p53-KQ* mouse model, our study demonstrates that p53-mediated transcription and tumor suppression can be activated by acetylation *in vivo* in the absence of robust p53 stabilization. Consistent with this notion, our recent study showed that the acetylation of C-terminal lysine residues induces p53 activation through blocking the interactions of p53 with transcriptional corepressors such as SET without affecting its stability (10). Moreover, knockout of *set* in mouse results in activation of p53 target genes without apparent increase of p53 protein levels, and embryonic lethality of *set* knockout mice can be partially rescued by concomitant deletion of *p53* (22). Notably, in contrast to the $p53^{KQ/KQ}$ mice, which died soon after birth due to insufficient brain development, the $p53^{KQ/-}$ mice developed normally during embryonic stages after reducing p53-KQ protein levels by half. Thus, although p53 stabilization is not absolutely required for its activation and tumor suppression, our data support the importance of the protein levels in p53

activation and emphasizes that the levels of the p53 protein are critical for the severity of the phenotypes caused by p53 activation.

There has been much interest in understanding how p53 is activated with the goal of using the diverse regulatory mechanisms to find novel therapeutic strategies to combat cancer. Because the activation of p53 often leads to terminal consequences such as cell death and senescence, p53 is critically regulated through posttranslational modification to repress its activities. For example, the binding of Mdm2/MdmX can inhibit p53 activities by ubiquitination-mediated protein degradation and by transcriptional repression. Similarly, the binding of SET to the unacetylated p53 CTD represses p53 transcriptional activity by blocking the recruitment of coactivators. Counteracting these repression mechanisms presents potential ways to activate p53. Mdm2 inhibitor Nutlin achieves p53 activation through disruption of the binding between Mdm2 and p53 N-terminus. Moreover, recent studies showed that the deletion of p53 C terminus in mice results in the activation of p53 and premature lethality (7,8). Our study showed that the acetylation mimicking $p53^{KQ/-}$ mice resulted in p53 activation and tumor suppression, raising an interesting possibility for activating p53 function in human cancers without increasing protein levels.

The p53 protein is known as the “guardian of the genome” because of its crucial role in coordinating cellular responses to genotoxic stress. Stabilization of p53 has been well accepted as a “hallmark” for the DNA damage response. Although the roles of p53 in both tumor suppression and DNA damage responses are indisputable, the critical issue is whether p53 executes its tumor suppressive function in the manner reminiscent of the DNA damage response. By using a mouse model in which p53 status can be reversibly switched *in vivo* between functional and inactive states, Christophorou et al. showed that the p53-mediated DNA damage response is irrelevant for suppression of radiation-induced lymphoma (23). In contrast, delaying the restoration of p53 function until the acute radiation response has subsided abrogates all of the radiation-induced pathology yet preserves much of the protection from lymphoma (23). Moreover, by somatically deleting p53 in the tissues of mice at various stages, Hinkal et al. found that the absence or presence of p53 during IR treatment had no effect on radiation-induced lymphoma latency (24), confirming that the immediate p53 damage response was irrelevant for cancer prevention. Consistent with this notion, both p53–3KR and $p53^{25,26}$ are severely compromised in DNA damage responses but their tumor suppressor function remains largely intact (6,25). On the other hand, Mdm2 acts as a major inhibitor of p53 by inducing its degradation. Through nearly two decades of intense research, a number of highly potent small-molecule inhibitors and peptides that inhibit the MDM2–p53 interaction (also called Mdm2 inhibitors) have been successfully developed (20). Like many DNA damage reagents, Mdm2 inhibitors are very effective in stabilizing p53 and activating p53 function. Nevertheless, none of them has been approved therapeutically effective in the clinical trials because of the dose-limiting toxicity (26). Thus, additional targets aiming at the p53 pathway are clearly needed. Our study suggests that targeting p53 acetylation at the CTD is a promising approach to activate its tumor suppression.

Supplementary Material

Refer to Web version on PubMed Central for supplementary material.

Acknowledgements

This work was supported by the National Cancer Institute of the National Institutes of Health under Award 5R01CA216884, 5R01CA190477, 5R01CA085533 and 5RO1CA224272 to W.G. The content is solely the responsibility of the authors and does not necessarily represent the official views of the National Institutes of Health.

References

1. Hu W, Feng Z, Levine AJ. The Regulation of Multiple p53 Stress Responses is Mediated through MDM2. Genes Cancer 2012;3:199–208 [PubMed: 23150753]
2. Zhang Q, Zeng SX, Lu H. Targeting p53-MDM2-MDMX loop for cancer therapy. Sub-cellular biochemistry 2014;85:281–319 [PubMed: 25201201]
3. Kaiser AM, Attardi LD. Deconstructing networks of p53-mediated tumor suppression in vivo. Cell Death Differ 2018;25:93–103 [PubMed: 29099489]
4. Gu W, Roeder RG. Activation of p53 sequence-specific DNA binding by acetylation of the p53 C-terminal domain. Cell 1997;90:595–606 [PubMed: 9288740]
5. Luo J, Su F, Chen D, Shiloh A, Gu W. Deacetylation of p53 modulates its effect on cell growth and apoptosis. Nature 2000;408:377–81 [PubMed: 11099047]
6. Li T, Kon N, Jiang L, Tan M, Ludwig T, Zhao Y, et al. Tumor suppression in the absence of p53-mediated cell-cycle arrest, apoptosis, and senescence. Cell 2012;149:1269–83 [PubMed: 22682249]
7. Simeonova I, Jaber S, Draskovic I, Bardot B, Fang M, Bouarich-Bourimi R, et al. Mutant mice lacking the p53 C-terminal domain model telomere syndromes. Cell Rep 2013;3:2046–58 [PubMed: 23770245]
8. Hamard PJ, Barthelery N, Hogstad B, Mungamuri SK, Tonnessen CA, Carvajal LA, et al. The C terminus of p53 regulates gene expression by multiple mechanisms in a target- and tissue-specific manner in vivo. Genes Dev 2013;27:1868–85 [PubMed: 24013501]
9. Cai W, Su L, Liao L, Liu ZZ, Langbein L, Dulaimi E, et al. PBRM1 acts as a p53 lysine-acetylation reader to suppress renal tumor growth. Nature communications 2019;10:5800
10. Wang D, Kon N, Lasso G, Jiang L, Leng W, Zhu WG, et al. Acetylation-regulated interaction between p53 and SET reveals a widespread regulatory mode. Nature 2016;538:118–22 [PubMed: 27626385]
11. Wang D, Kon N, Tavana O, Gu W. The “readers” of unacetylated p53 represent a new class of acidic domain proteins. Nucleus 2017;8:360–9 [PubMed: 28406743]
12. Gromley A, Churchman ML, Zindy F, Sherr CJ. Transient expression of the Arf tumor suppressor during male germ cell and eye development in Arf-Cre reporter mice. Proc Natl Acad Sci U S A 2009;106:6285–90 [PubMed: 19339492]
13. Hingorani SR, Petricoin EF, Maitra A, Rajapakse V, King C, Jacobetz MA, et al. Preinvasive and invasive ductal pancreatic cancer and its early detection in the mouse. Cancer Cell 2003;4:437–50 [PubMed: 14706336]
14. Jacks T, Remington L, Williams BO, Schmitt EM, Halachmi S, Bronson RT, et al. Tumor spectrum analysis in p53-mutant mice. Current biology : CB 1994;4:1–7 [PubMed: 7922305]
15. McGowan KA, Li JZ, Park CY, Beaudry V, Tabor HK, Sabnis AJ, et al. Ribosomal mutations cause p53-mediated dark skin and pleiotropic effects. Nat Genet 2008;40:963–70 [PubMed: 18641651]
16. Cicalese A, Bonizzi G, Pasi CE, Faretta M, Ronzoni S, Giulini B, et al. The tumor suppressor p53 regulates polarity of self-renewing divisions in mammary stem cells. Cell 2009;138:1083–95 [PubMed: 19766563]
17. Yan H, Solozobova V, Zhang P, Armant O, Kuehl B, Brenner-Weiss G, et al. p53 is active in murine stem cells and alters the transcriptome in a manner that is reminiscent of mutant p53. Cell death & disease 2015;6:e1662

18. Adelman CA, Lolo RL, Birkbak NJ, Murina O, Matsuzaki K, Horejsi Z, et al. HELQ promotes RAD51 paralogue-dependent repair to avert germ cell loss and tumorigenesis. Nature 2013;502:381–4 [PubMed: 24005329]
19. Midgley CA, Desterro JM, Saville MK, Howard S, Sparks A, Hay RT, et al. An N-terminal p14ARF peptide blocks Mdm2-dependent ubiquitination in vitro and can activate p53 in vivo. Oncogene 2000;19:2312–23 [PubMed: 10822382]
20. Weber JD, Taylor LJ, Roussel MF, Sherr CJ, Bar-Sagi D. Nucleolar Arf sequesters Mdm2 and activates p53. Nature cell biology 1999;1:20–6 [PubMed: 10559859]
21. Honda R, Yasuda H. Association of p19(ARF) with Mdm2 inhibits ubiquitin ligase activity of Mdm2 for tumor suppressor p53. EMBO J 1999;18:22–7 [PubMed: 9878046]
22. Kon N, Wang D, Gu W. Loss of SET reveals both the p53-dependent and the p53-independent functions in vivo. Cell death & disease 2019;10:237 [PubMed: 30858352]
23. Christophorou MA, Ringshausen I, Finch AJ, Swigart LB, Evan GI. The pathological response to DNA damage does not contribute to p53-mediated tumour suppression. Nature 2006;443:214–7 [PubMed: 16957739]
24. Hinkal G, Parikh N, Donehower LA. Timed somatic deletion of p53 in mice reveals age-associated differences in tumor progression. PloS one 2009;4:e6654
25. Brady CA, Jiang D, Mello SS, Johnson TM, Jarvis LA, Kozak MM, et al. Distinct p53 transcriptional programs dictate acute DNA-damage responses and tumor suppression. Cell 2011;145:571–83 [PubMed: 21565614]
26. Wang S, Zhao Y, Aguilar A, Bernard D, Yang CY. Targeting the MDM2-p53 Protein-Protein Interaction for New Cancer Therapy: Progress and Challenges. Cold Spring Harbor perspectives in medicine 2017;7

Significance:

Although robust p53 stabilization is critical for acute p53 responses such as DNA damage, this study underscores the important role of low basal p53 protein levels in p53 activation and tumor suppression.

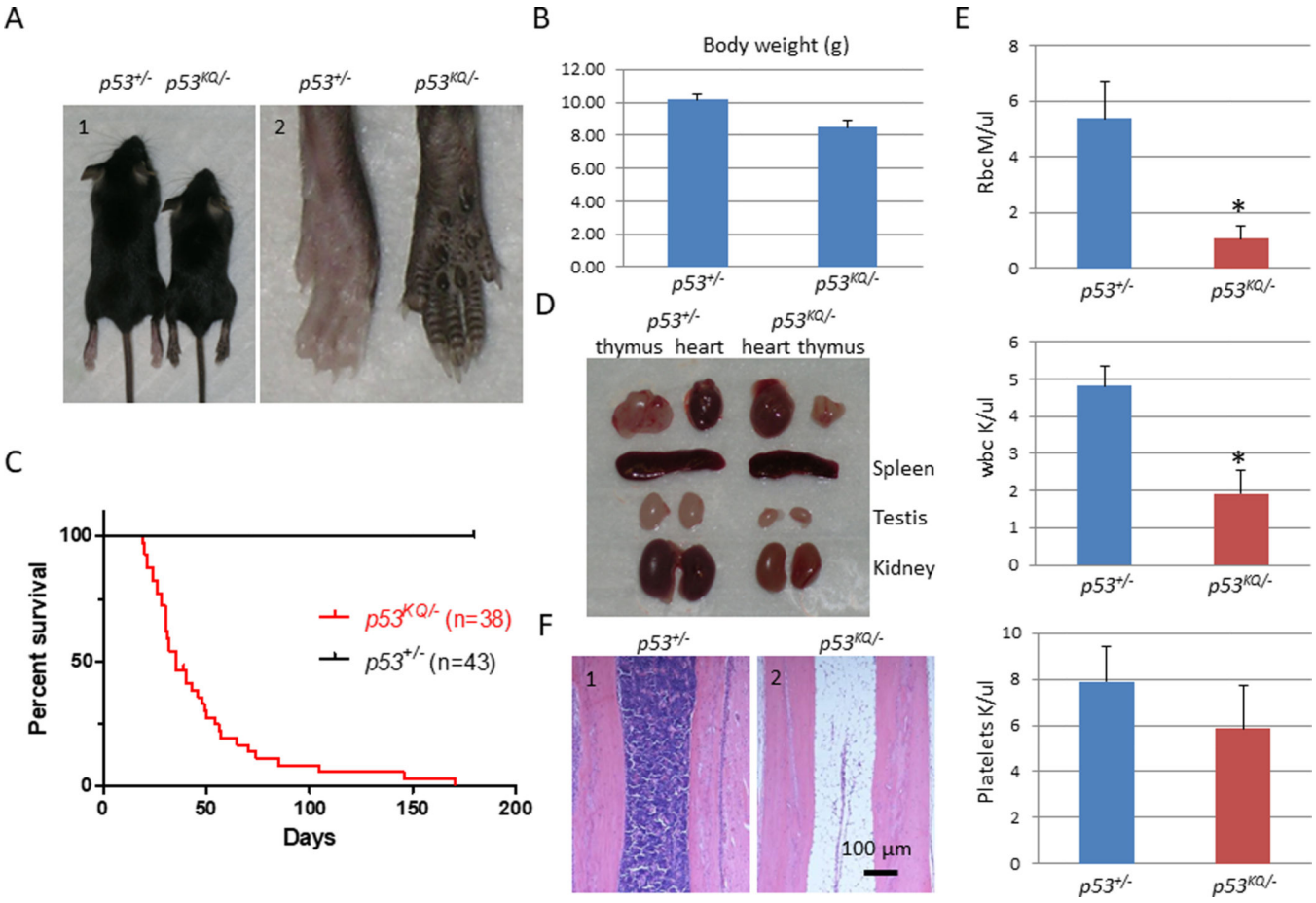

Figure 1.

p53$^{KQ/-}$ mice died prematurely due to anemia. **A**, 1, Gross appearance of the weaning age *p53*$^{+/-}$ and *p53*$^{KQ/-}$ mice; 2, an enlarged picture to highlight the hyperpigmentation on the paw of *p53*$^{KQ/-}$ mice. **B**, Body weight comparison between *p53*$^{+/-}$ and *p53*$^{KQ/-}$ mice. **C**, Kaplan-Meier plot of the survival curves for *p53*$^{+/-}$ and *p53*$^{KQ/-}$ mice. **D**, Comparison of internal organs of *p53*$^{+/-}$ and *p53*$^{KQ/-}$ mice. **E**, Complete blood cell count of three-week-old *p53*$^{+/-}$ and *p53*$^{KQ/-}$ mice. *: p<0.05. **F**, Representative H&E staining of the bone sections from *p53*$^{+/-}$ and morbid-bound *p53*$^{KQ/-}$ mice.

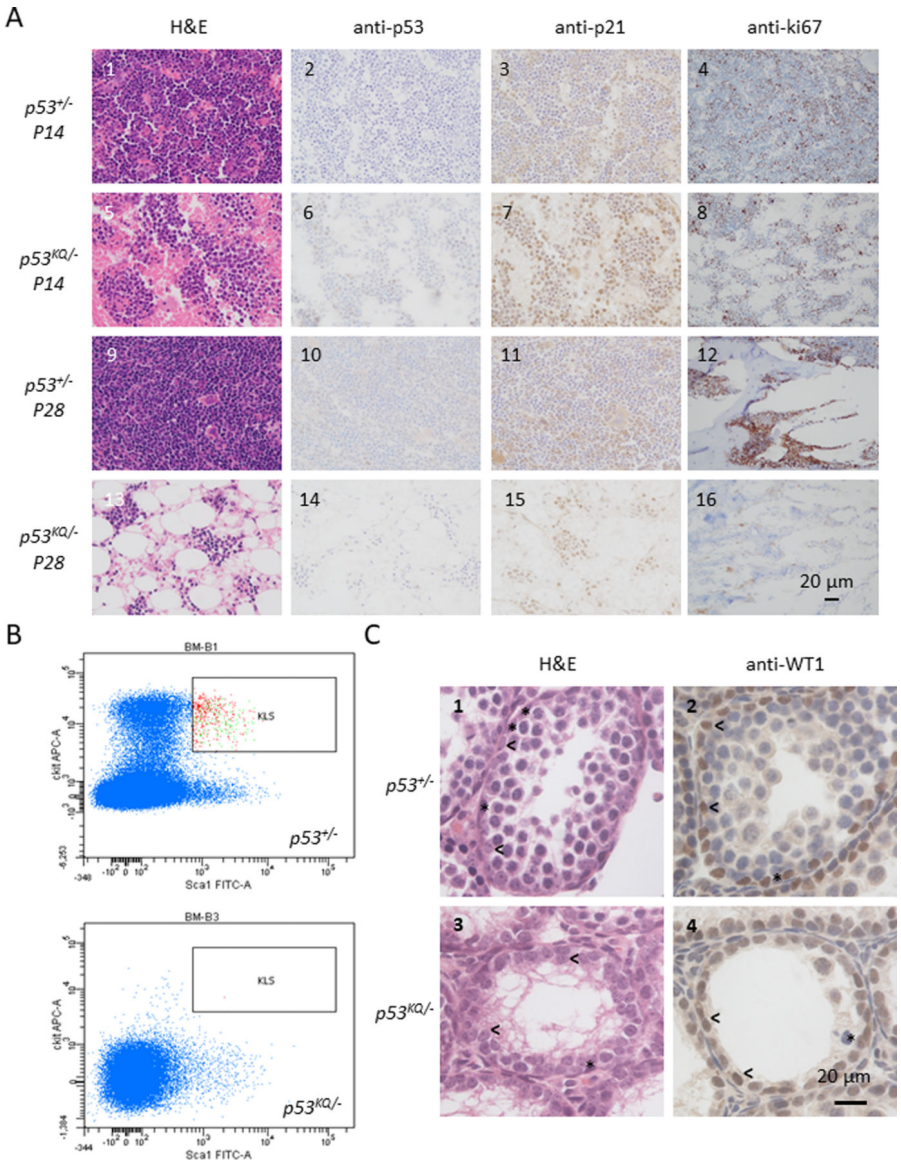

Figure 2.

Progressive depletion of bone marrow cells in *p53*$^{KQ/-}$ mice. **A**, Histological analysis of bone sections from *p53*$^{+/-}$ (panel 1–4, and 9–12) and *p53*$^{KQ/-}$ (panel 5–8 and 13–16) mice at postnatal day 14 (panel 1–8) and P28 (panel 9–16). Bone sections were processed for H&E staining (panels 1, 5, 9, and 13), immunostained with anti-p53 antibody (panel 2, 6, 10, and 14), anti-p21 antibody (panel 2, 7, 11, and 15), and anti-ki67 antibody (panel 4, 8, 12, and 16). **B**, FACS analysis of bone marrow cells gated on Lin^{-} cells to determine the population of the hematopoietic stem cells (Lin^{-}Sca-1^{+}cKit^{+}) in *p53*$^{+/-}$ and *p53*$^{KQ/-}$ mice. **C**, Defective spermatogenesis in *p53*$^{KQ/-}$ mice. Representative pictures of the testis from three-week-old *p53*$^{+/-}$ (1 and 2) and *p53*$^{KQ/-}$ (3 and 4) mice. 1 and 3: H&E staining; 2 and 4: Immunostaining using antibody against WT1. WT1-staining-positive cells (with brown-colored nuclei) are Sertoli cells. * indicates spermatogonia; < indicates Sertoli cells.

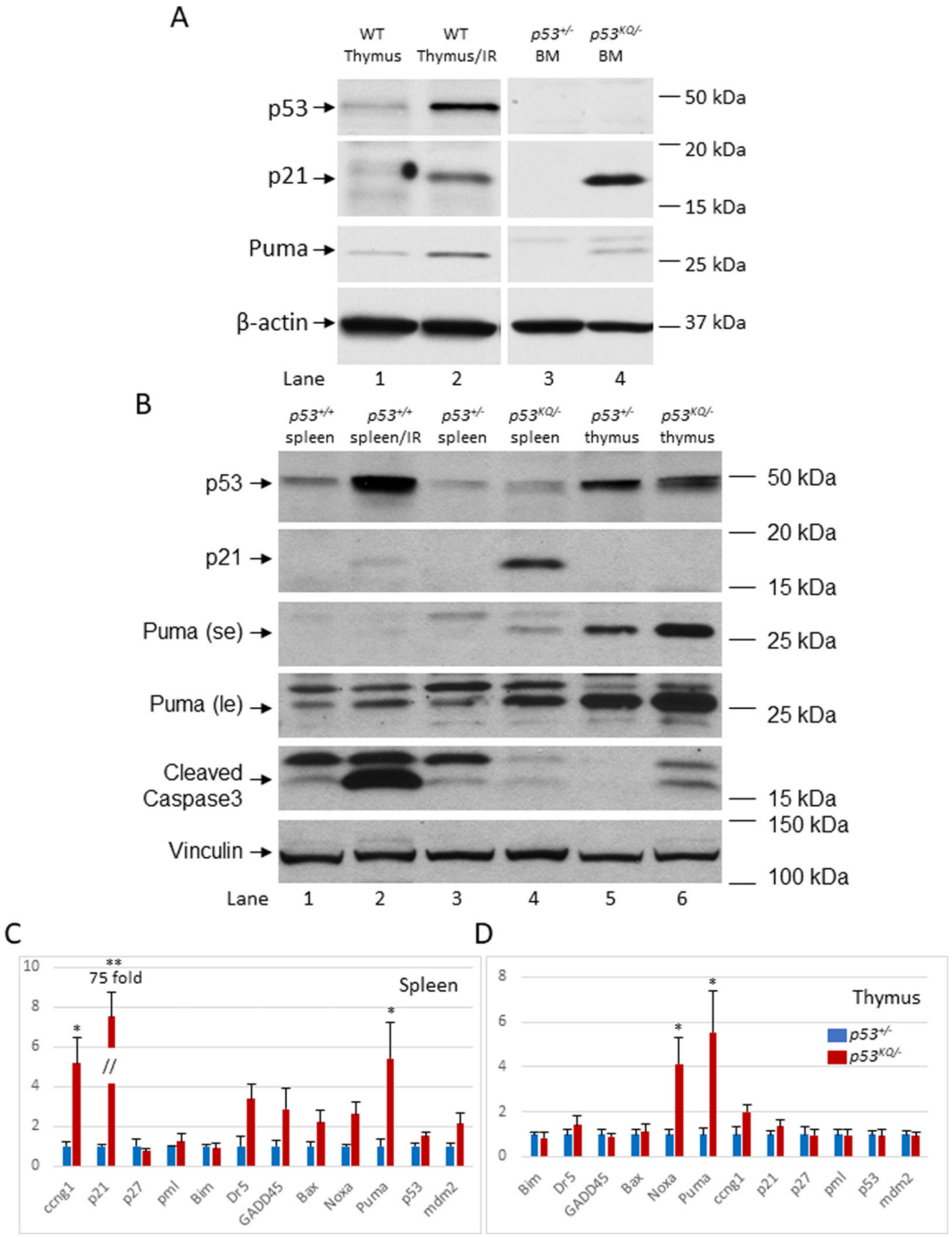

Figure 3.

Activation of p53 target genes. **A**, Expression of p53 target genes in bone marrow cells from P6 $p53^{+/-}$ (lane 3) and $p53^{KQ/-}$ (lane 4) mice was determined by Western blotting analysis. Total protein extracts of thymus from an untreated (lane 1) and an IR-treated (lane 2) wild type mice were used as controls. After the proteins were transferred, the blot was probed with antibodies against p53, p21, puma, and β-actin, respectively. IR: ionizing radiation; BM: bone marrow. **B**, Western blot analysis to determine the expression levels of p53, puma and p21, and the levels of apoptosis marker, cleaved Caspase 3. The protein extracts from

the spleens of an untreated (lane 1) and IR-treated (lane 2) wild type mice were used as controls. The protein extracts from the spleen (lane 3) and thymus (lane 5) of a $p53^{+/-}$ mouse, and the protein extracts from the spleen (lane 4) and thymus (lane 6) of a $p53^{KQ/-}$ mouse were tested. **C**, Real-time PCR (RT-PCR) assays were performed to determine the relative expression levels of p53 target genes in the spleens from $p53^{+/-}$ and $p53^{KQ/-}$ mice. *: $p<0.05$, **: $p<0.001$. **D**, RT-PCR assays were performed to determine the relative expression levels of p53 target genes in the thymi from $p53^{+/-}$ and $p53^{KQ/-}$ mice. *: $p<0.05$.

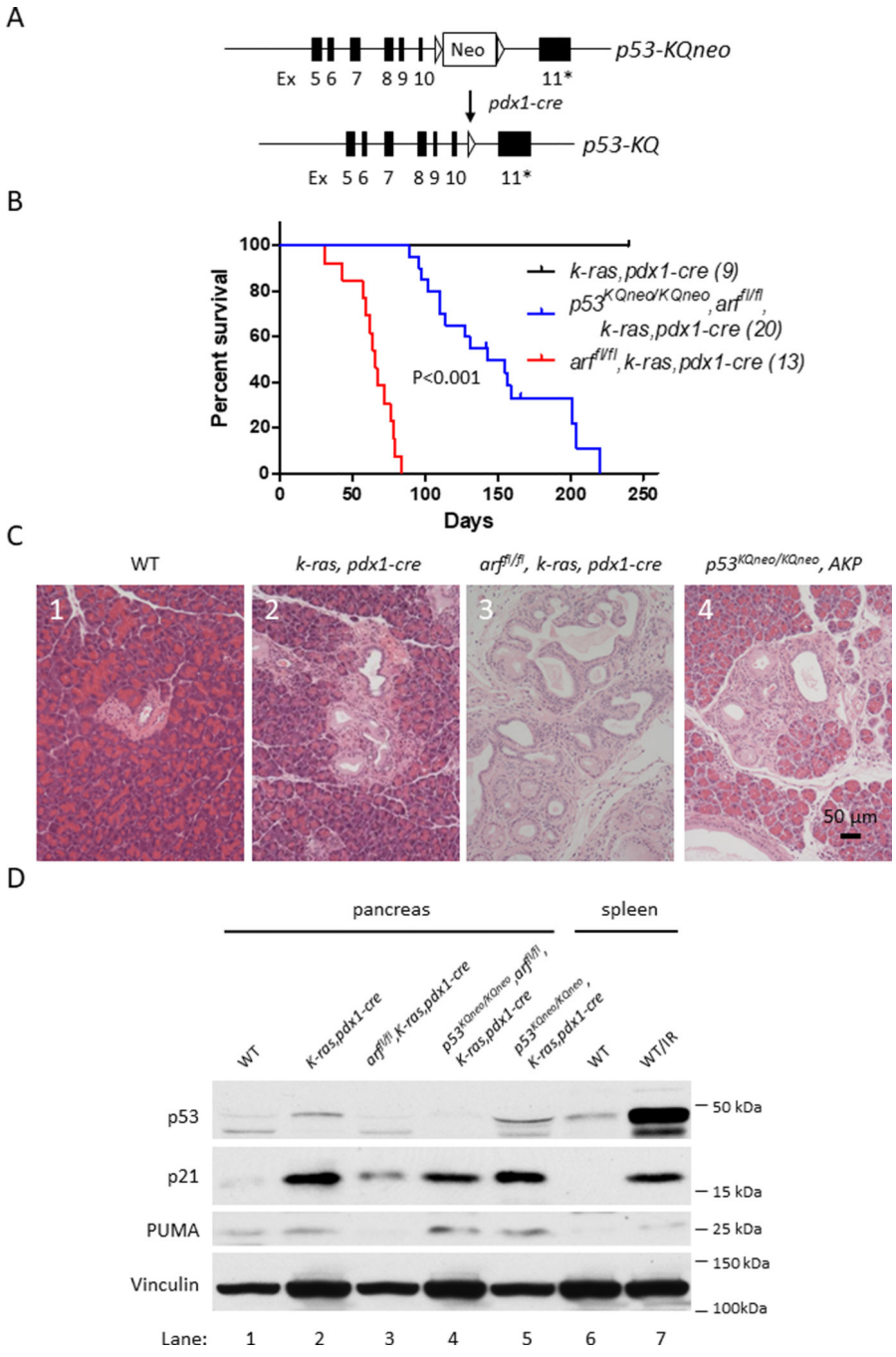

Figure 4.

Expression of p53-KQ mutant proteins extended the life-span of a PDAC mouse model. **A**, Schematic diagram of conditional expression of *p53-KQ* mutant in pancreas. The *neomycin* cassette contained in the *p53-KQneo* allele is removed upon the expression of *pdx1-cre* to restore the splicing between exon 10 and exon 11, and to allow the expression of p53-KQ mutant in pancreas. 11*: indicating the exon 11 containing all seven K-to-Q mutations. **B**, Kaplan-Meier survival curve for pancreatic ductal adenocarcinoma mouse models with various *arf* and *p53* genotypes. **C**, Representative pictures of pancreas, stained with

hematoxylin and eosin, from 1: wild type mouse; 2: *k-ras,pdx1-cre* mouse (KP); 3: $arf^{fl/fl}$,*k-ras,pdx1-cre* mouse (AKP); and 4: $p53^{KQneo/KQneo}$,$arf^{fl/fl}$,*k-ras,pdx1-cre* mouse. **D.** Western blot analysis of the protein extracts from the PDAC tumors from mice with various genotypes as indicated. WT: wild type pancreas. The blot was probed with anti-p53, anti-p21, and anti-PUMA antibodies. The protein extracts from wild type spleen of an untreated or IR-treated mouse were used to show the expression of p53, p21, and puma proteins. The levels of Vinculin was used as protein loading control.